

Mechanical Stress Identification Method in Anisotropic Ferromagnetic Materials Using Eddy Current Testing

Safae Bouterfas^{ID}, Yann Le Bihan^{ID}, Laurent Santandrea, and Laurent Daniel^{ID}

Laboratoire de Génie Électrique et Électronique de Paris, CentraleSupélec, CNRS, Université Paris-Saclay, 91192 Gif-sur-Yvette, France

Laboratoire de Génie Électrique et Électronique de Paris, CNRS, Sorbonne Université, 75252 Paris, France

This work presents an identification method for multi-axial stresses in steel pipelines. The proposed electromagnetic non-destructive technique evaluates the impedance variation of an eddy current (EC) sensor. The method applies to ferromagnetic materials, including anisotropic ones. It is a model-based approach using a finite-element model (FEM) that incorporates the magneto-elastic behavior of the material and simulates the variation of the EC sensor impedance with stress. Four parameters are needed to describe the material behavior. Although the magnetic parameters used in the numerical model are identified from anhysteretic measurements, the results of the identification method correlate with experiments performed on samples extracted along two orthogonal directions of a pipeline.

Index Terms—Anisotropy, API-5L X52, coupled problem, eddy current (EC) non-destructive testing (NDT), magneto-elasticity, multi-scale model, steel pipeline.

I. INTRODUCTION

EDDY current (EC) non-destructive testing (NDT) is widely used to detect defects and inspect the integrity of metallic structures [1]. It can also be used to evaluate in real-time stress induced by mechanical loading, for example, in pipelines. The technique exploits the change in electrical or magnetic properties due to stress [2]. In the case of ferromagnetic materials, the variation of electrical conductivity due to stress [3] can be neglected compared to that of magnetic permeability [4]. The general principle of the proposed technique is that the effect of stress on magnetic permeability is reflected in the measured impedance signal from an EC sensor. This technique was applied to isotropic ferromagnetic material under uniaxial stress in [5] and similarly in [6] for cylindrical bars. Another use of EC NDT for stress evaluation in isotropic ferromagnetic materials is proposed in [7] based on phase shift detection.

This article is dedicated to the application of an EC technique to detect internal stresses in anisotropic ferromagnetic materials, such as the API-5L X52 low-carbon steel used in gas pipelines. A magneto-elastic behavioral law for anisotropic ferromagnetic material is detailed, along with its parameter identification method. Then, its output, the magnetic properties, is implemented in a magneto-dynamic finite-element model (FEM) of a U-shaped EC sensor. The impedance change in the sensor is compared to experimental results.

II. MATERIAL MODEL

A simplified multi-scale model (SMSM) [8] is used to describe the macroscopic anhysteretic magnetic behavior of

Manuscript received 6 November 2022; revised 3 January 2023; accepted 8 January 2023. Date of publication 23 January 2023; date of current version 25 April 2023. Corresponding authors: S. Bouterfas; L. Daniel (e-mail: safae.bouterfas@gmail.com; laurent.daniel@centralesupelec.fr).

Color versions of one or more figures in this article are available at <https://doi.org/10.1109/TMAG.2023.3237316>.

Digital Object Identifier 10.1109/TMAG.2023.3237316

0018-9464 © 2023 IEEE. Personal use is permitted, but republication/redistribution requires IEEE permission. See <https://www.ieee.org/publications/rights/index.html> for more information.

ferromagnetic materials under stress. The material is described as a collection of magnetic domains with orientation α (unit vector). Each domain is characterized by its magnetization \mathbf{M}_α and magnetostriction strain tensor $\boldsymbol{\varepsilon}_\alpha^\mu$

$$\mathbf{M}_\alpha = M_s \boldsymbol{\alpha} \quad (1)$$

$$\boldsymbol{\varepsilon}_\alpha^\mu = \frac{3}{2} \lambda_s \left(\boldsymbol{\alpha} \otimes \boldsymbol{\alpha} - \frac{1}{3} \mathbf{I} \right) \quad (2)$$

where M_s and λ_s are the saturation magnetization and the saturation magnetostriction constant of the material, respectively. \otimes is the tensor product and \mathbf{I} is the second-order identity tensor. The free energy W_α for a given orientation α is defined as the sum of three energy terms: the magneto-static energy W_α^{mag} , the magneto-elastic energy W_α^{el} , and the anisotropy energy W_α^{an}

$$W_\alpha = W_\alpha^{\text{mag}} + W_\alpha^{\text{el}} + W_\alpha^{\text{an}} \quad (3)$$

$$W_\alpha^{\text{mag}} = -\mu_0 \mathbf{H} \cdot \mathbf{M}_\alpha \quad (4)$$

$$W_\alpha^{\text{el}} = -\mathbf{T} : \boldsymbol{\varepsilon}_\alpha^\mu \quad (5)$$

$$W_\alpha^{\text{an}} = -J (\boldsymbol{\beta} \cdot \boldsymbol{\alpha})^2 \quad (6)$$

where \mathbf{H} is the applied magnetic field and \mathbf{T} is the applied stress. μ_0 is the vacuum magnetic permeability ($\mu_0 = 4\pi \cdot 10^{-7} \text{ H}\cdot\text{m}^{-1}$). J is an anisotropy constant and $\boldsymbol{\beta}$ is the anisotropy direction (unit vector).

An internal variable f_α is introduced, representing the volume fraction of a domain with orientation α :

$$f_\alpha = \frac{\exp(-A_s W_\alpha)}{\int_\alpha \exp(-A_s W_\alpha)}. \quad (7)$$

Here, A_s is a material parameter given by $A_s = 3\chi^0/(\mu_0 M_s^2)$, where χ^0 is the initial magnetic susceptibility of the material under no applied stress. The macroscopic magnetization \mathbf{M} is finally calculated by integration over all the possible orientations α

$$\mathbf{M} = M_s \int_\alpha f_\alpha \boldsymbol{\alpha} d\alpha. \quad (8)$$

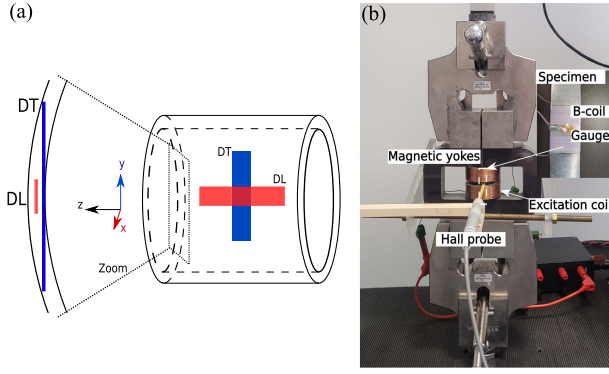


Fig. 1. (a) Schematic of the cut-out samples and (b) experimental bench for magneto-elastic characterization.

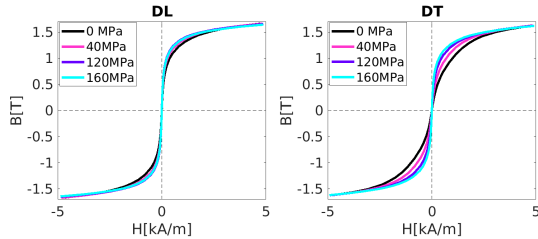


Fig. 2. Measured anhysteretic curves for API-5L X52 under uniaxial stress.

The anisotropic SMSM then relies on only four material parameters: M_s , λ_s , J , and χ^0 .

A. Parameter Identification

In order to apply the SMSM to API-5L X52, ferromagnetic steel used for gas pipelines, two samples labeled DL and DT were extracted in the longitudinal (DL) and the transverse (DT) directions of a pipe [Fig. 1(a)]. A magneto-elastic characterization bench [Fig. 1(b)] is used to assess the material behavior and identify the model parameters. The setup allows for measuring the magnetization curve of samples subjected to the magnetic field and uniaxial stress applied parallel to the magnetic field. The results are shown in Fig. 2. From the modeling point of view, due to the anisotropy of the behavior, the initial magnetic susceptibility χ^0 is an equivalent scalar fit on measurements under no stress from the DL and DT samples (plain symbols in Fig. 3). J is fit to ensure that the initial values of the magnetic permeability (under no applied stress) are correct for both directions. β is parallel to DL (direction with the highest magnetic permeability). The material parameters identified for API-5L X52 are given in Table I.

B. Definition of the Anhysteretic Permeability Tensor

Once the material parameters are known, the SMSM allows computing the constitutive response of the material $\mathbf{B}(\mathbf{T}, \mathbf{H}) = \mu_0(\mathbf{M}(\mathbf{T}) + \mathbf{H})$ under any magneto-mechanical loading. The corresponding magnetic permeability can be deduced using (9). Assuming the magnetic permeability tensor to be diagonal, the anhysteretic magnetic permeability can be defined in the form of (10), where μ_{xx} , μ_{yy} , and μ_{zz} are

TABLE I

SMSM MATERIAL PARAMETERS FOR API-5L X52

Parameter	M_s	χ^0	λ_s	J
Value	$1.33 \cdot 10^6$	3750	$6.0 \cdot 10^{-6}$	555
Unit	$\text{A}\cdot\text{m}^{-1}$	-	-	$\text{J}\cdot\text{m}^{-3}$

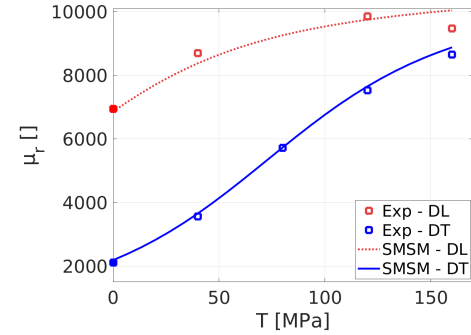


Fig. 3. Low-field anhysteretic magnetic permeability of API-5L X52 along DL and DT under uniaxial stress, applied along the magnetization direction. The plain symbols indicate the measurement data used for the identification of material parameters.

obtained by applying the magnetic field along the directions \mathbf{x} , \mathbf{y} , and \mathbf{z} , respectively,

$$\mu_r(\mathbf{T}) = \frac{(\mathbf{M} + \mathbf{H}) \cdot \mathbf{H}}{\mathbf{H} \cdot \mathbf{H}} \quad (9)$$

$$\bar{\bar{\mu}}(\mathbf{T}) = \text{diag}(\mu_{xx}(\mathbf{T}), \mu_{yy}(\mathbf{T}), \mu_{zz}(\mathbf{T})). \quad (10)$$

An experimental anhysteretic magnetic permeability is deduced using the $B(H)$ anhysteretic curves at low field ($\pm 10 \text{ A}\cdot\text{m}^{-1}$) from Fig. 2. A comparison between experimental and modeling results is shown in Fig. 3 for the relative permeability μ_r . Plain symbols have been used to show the data used for the identification of material parameters, while continuous lines show model prediction. It is visible that the SMSM allows a satisfying description of both initial and stress-induced anisotropies.

III. MAGNETO-DYNAMIC NUMERICAL MODEL

Assuming that the effect of stress on the magnetic permeability at the low field is analogous to its effect on the anhysteretic permeability and that the linear approximation is valid, a linear elasto-magneto-dynamic FEM is defined using the permeability tensor $\bar{\bar{\mu}}(\mathbf{T})$ under stress computed with the SMSM. The magnetic vector potential formulation is used to solve the magneto-dynamic equation in the frequency domain (11), and the Dirichlet boundary condition is applied on the external surface of the study domain. The coils of the EC sensor are defined as homogenized multi-turn coils

$$\nabla \times (\boldsymbol{\mu}^{-1} \times \mathbf{A} + \sigma j \omega \mathbf{A}) = \mathbf{J}_e \quad (11)$$

where \mathbf{A} is the magnetic potential vector and \mathbf{J}_e is the excitation current. A coil geometry analysis is used to compute the current flow of the coil and then an iterative solver is used to solve (11).

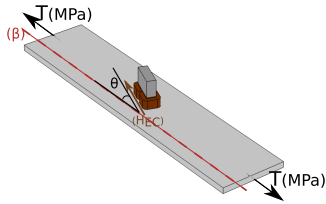


Fig. 4. Sensor configuration on the DL sample.

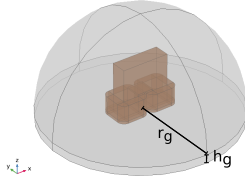


Fig. 5. Geometry of the magneto-dynamic FEM.

A. Model Geometry

The geometry of the EC sensor consists of a U-shaped magnetic core with overall dimensions $4 \times 2 \times 3 \text{ mm}^3$. Two identical square coils with N_c turns, and a cross section of $1 \times 0.45 \text{ mm}$ are mounted in series at the ends of the magnetic core as shown in Fig. 4. The material geometry is represented by a cylinder with a radius r_g and a height h_g (Fig. 5). The material thickness h_g is reduced to being six times the skin depth δ because the joule losses, from EC, remain unchanged for more significant h_g

$$\delta = \frac{1}{\sqrt{\sigma \mu_0 \mu_r \pi f}} \quad (12)$$

where f is the frequency, and σ and μ_r are the electrical conductivity and the relative magnetic permeability of the material, respectively. The shape of the EC sensor makes it sensitive not only to changes in magnetic properties due to stress, but also to the initial anisotropy. The angle θ defines the sensor orientation with respect to the anisotropy direction β . In the case of DL samples shown below, β coincides with the direction of the uniaxial stress (see Fig. 4). When the sensor direction is parallel to β , the angle θ is then zero.

B. Mesh Strategy

The FEM model is built to generate 2-D maps of the impedance variation for bi-axial stress up to $\pm 200 \text{ MPa}$ in the sample plane. As shown in Fig. 3, the anisotropic magnetic permeability exhibits high variations in a stress range from 0 to 160 MPa. At an operating frequency of 500 kHz, the skin depth δ under these stress levels varies from $\delta_{\min} = 3.1 \mu\text{m}$ to $\delta_{\max} = 12.6 \mu\text{m}$. Adapting the mesh to the value of δ adds significant numerical noise to the computed impedance values. Hence, a constant mesh, supporting the full range of δ variations, is adopted.

A challenge for the 3-D FEM is to obtain acceptable accuracy with minimum computational load (memory and time). The final problem contains 380000 degrees of freedom using quadratic tetrahedral and prismatic edge elements. Nevertheless, refining the mesh in zones with high-energy gradients is recommended. In a magneto-dynamic problem,

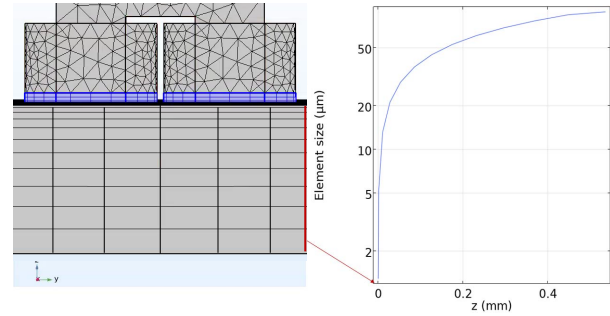


Fig. 6. Size evolution of prismatic elements in the normal direction of the sample.

these zones are located around the coil and in the skin depth of the material. In this study, the used physical parameters give a small skin depth compared to the geometrical dimensions. To address this geometry constraint, prismatic elements are chosen to mesh this zone [9] as well as the air gap between the sensor and the material. These elements are efficient for field calculation in boundary layers. The sweep parameters of the prismatic layers (Fig. 6) are the thickness of the first layer U_1 , the growth rate Sf , and the number of layers N_l . These parameters are chosen to have two layers in δ_{\min} and a total of 12 layers in h_g ($6 \delta_{\max}$). In order to avoid changing the mesh when changing the sensor position, it was chosen to keep the full meshed constant and to rotate the material property $\overline{\mu}(\mathbf{T})$ under the sensor, using a rotation matrix $\overline{\mathbf{R}}$, around the normal direction

$$\overline{\mu}(\mathbf{T}, \theta) = \overline{\mathbf{R}}(\theta) \cdot \overline{\mu}(\mathbf{T}) \cdot \overline{\mathbf{R}}(\theta)^t. \quad (13)$$

C. Model Calibration

The electrical conductivity σ of the material is used as an adjustment parameter to approximate the frequency for maximum impedance variation obtained experimentally from the sensor placed on a sample. The lift-off (Lo , the distance between the EC sensor and the material surface) is another adjustment parameter set so as to approximate the value of the measured impedance under no applied stress. The first step of the model calibration is to use the electrical conductivity σ ($5.38 \cdot 10^6 \text{ S}\cdot\text{m}^{-1}$) measured by a four-point probes method for a static excitation. The model frequency for a maximum impedance variation (f_{FEM}) is different from the experimental frequency ($f_{\max} = 500 \text{ kHz}$). However, when the material electrical conductivity is raised to 7σ , the model frequency is $f_{\text{FEM}} \approx f_{\max}$. Then Lo is adjusted to fit the computed impedance module to measurements.

IV. RESULTS

Using the parameters in Table II, a computation for $\theta = 0$ and $f = 500 \text{ kHz}$ gives an impedance module of 3730Ω for 3820Ω in the experiment. The magnetic field loops are mainly channeled in the magnetic yoke and the air domain surrounding the EC sensor.

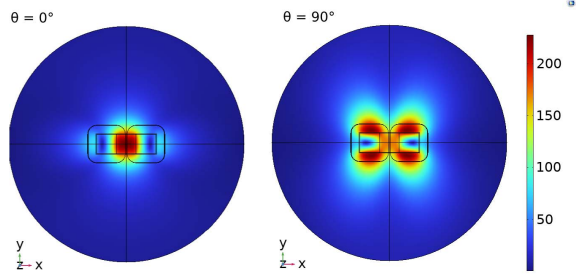


Fig. 7. Magnetic flux density distribution B(mT) for two sensor orientations.

TABLE II

FEM PARAMETERS FOR API-5L X52

Parameter	N_c	I_{coil}	σ	L_o	r_g	h_g	N_l	Sf
Value	215	128	$38 \cdot 10^6$	140	15	76	12	17
Unit	-	μA	$S \cdot m^{-1}$	μm	mm	μm	-	-

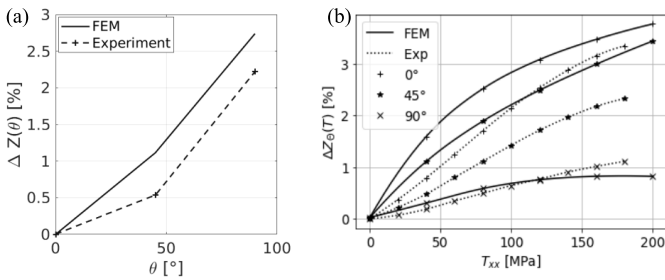


Fig. 8. Impedance change of the EC sensor at 500 kHz. (a) Impedance variation for different sensor orientations of an unstressed material. (b) Impedance variation for different uniaxial stresses along $\theta = 0$.

A. Initial Anisotropy Evaluation

For multiple sensor orientations, the magnetic density flux distribution changes. The EC area increases when the sensor is normal to the anisotropy direction (Fig. 7). Thanks to the sensor geometry, the anisotropy effect is detected. Fig. 8(a) shows a satisfactory agreement for the angular variation $\Delta Z(\theta)$ between the modeling and experimental results for different sensor orientations under no applied stress

$$\Delta Z(\theta) = \frac{|Z(\theta) - Z_{0^\circ}|}{X_{0^\circ}}. \quad (14)$$

Z_{0° and X_{0° are the impedance and the reactance, respectively, of the sensor placed at $\theta = 0$ on the unstressed material. $Z(\theta)$ is the impedance for an angle θ .

B. Stress-Induced Anisotropy Evaluation

To evaluate the stress effect on the impedance signal, a similar measurement output $\Delta Z_\theta(\%)$ is used

$$\Delta Z_\theta(\mathbf{T}) = \frac{|Z_\theta(\mathbf{T}) - Z_{0^\circ}|}{X_{0^\circ}}. \quad (15)$$

$Z_\theta(\mathbf{T})$ is the impedance of the sensor with material under stress \mathbf{T} and for an orientation θ . The model predicts the correct trends for the evolution of the EC sensor impedance under uniaxial stress (Fig. 8). However, the magnitude difference between the model and the experiment, on the strip samples,

can be partially explained by experimental uncertainties on the setup, for instance, the lift-off [10] or on the orientation of the sensor. Moreover, the magnetization state of the specimen was not taken into account in the model but it was present in the experiment. This method presents a good sensitivity to stress when the three orientations of the sensor are combined [Fig. 8(b)].

V. CONCLUSION

A combination of a simplified multi-scale model for magneto-elastic behavior with a magneto-dynamic finite-element simulation has been implemented. It allows for predicting the variations of the impedance of an EC sensor placed on an anisotropic ferromagnetic material subjected to mechanical stress. The strength of the approach is that it allows the implementation of both initial and stress-induced magnetic anisotropies using reasonable computational resources.

The model can be used to predict the EC sensor impedance for materials under bi-axial stress, such as in pipelines. Furthermore, 2-D impedance maps of the EC sensor for different orientations can be generated and used to solve an inverse problem for stress identification. The final goal of this study is to perform such an approach on pipelines subjected to internal pressure in order to estimate the levels of internal stress.

ACKNOWLEDGMENT

This work was supported by the Research and Innovation Center for Energy (RICE) of GRTGaz group, Villeneuve-la-Garenne, France.

REFERENCES

- [1] H. A. Sabbagh, R. K. Murphy, E. H. Sabbagh, J. C. Aldrin, and J. S. Knopp, *Computational Electromagnetics and Model-Based Inversion: A Modern Paradigm for Eddy-Current Nondestructive Evaluation* (Scientific Computation). New York, NY, USA: Springer, 2013.
- [2] F. Yu, M. P. Blodgett, and P. B. Nagy, "Eddy current assessment of near-surface residual stress in shot-peened inhomogeneous nickel-base superalloys," *J. Nondestruct. Eval.*, vol. 25, no. 1, pp. 16–27, Mar. 2006.
- [3] M. Morozov, G. Y. Tian, and P. J. Withers, "The pulsed eddy current response to applied loading of various aluminium alloys," *NDT & E Int.*, vol. 43, no. 6, pp. 493–500, 2010.
- [4] B. D. Cullity and C. D. Graham, *Introduction to Magnetic Materials*. Hoboken, NJ, USA: Wiley, 2011.
- [5] A. Dahia, E. Berthelot, Y. Le Bihan, and L. Daniel, "A model-based method for the characterisation of stress in magnetic materials using eddy current non-destructive evaluation," *J. Phys. D, Appl. Phys.*, vol. 48, no. 19, 2015, Art. no. 195002.
- [6] S. Abuku and B. D. Cullity, "A magnetic method for the determination of residual stress," *Exp. Mech.*, vol. 11, no. 5, pp. 217–223, May 1971.
- [7] M. S. García Alonso, A. Hernando, J. Vinolas, and M. A. García, "Magnetic detection of high mechanical stress in iron-based materials using eddy currents and phase shift measurements," *J. Appl. Phys.*, vol. 129, no. 24, Jun. 2021, Art. no. 243901.
- [8] L. Daniel, O. Hubert, and M. Rezik, "A simplified 3-D constitutive law for magnetomechanical behavior," *IEEE Trans. Magn.*, vol. 51, no. 3, pp. 1–4, Mar. 2015.
- [9] H. Zaidi, "Méthodologies pour la modélisation des couches fines et du déplacement en contrôle non destructif par courants de Foucault: Application aux capteurs souples," Ph.D. thesis, STITS Doctoral School, Université Paris Sud-Paris XI, Bures-sur-Yvette, France, 2012.
- [10] Y. Le Bihan, J. Pávó, and C. Marchand, "Study and experimental validation of the calculation of the ECT signal induced by a minute crack using a FEM-BIM combination," *NDT & E Int.*, vol. 39, no. 6, pp. 476–486, Sep. 2006.